Crystallization and melting in the Lennard-Jones system: Equilibration, relaxation, and long-time dynamics of the moving interface

H. L. Tepper[a] and W. J. Briels[b]
Computational Dispersion Rheology, University of Twente, P.O. Box 217, 7500 AE Enschede, The Netherlands

(Received 25 June 2001; accepted 6 September 2001)

Nonequilibrium molecular dynamics simulations have been carried out on the growth and melting of the Lennard-Jones (100) interface at small undercoolings and superheatings. Two regimes of linear growth rate were discovered: a short-time regime associated with interface relaxation and a long-time regime associated with the macroscopic limit of growth and melting. It was shown that, if system sizes or equilibration times are taken too small, one will find only the initial regime. On the basis of our very accurate results on the macroscopic growth rates close to equilibrium, the possibility of a discontinuity in the temperature dependence of growth and melting rates at the melting point was ruled out. © *2001 American Institute of Physics.* [DOI: 10.1063/1.1413972]

I. INTRODUCTION

Understanding the microscopic processes associated with crystal growth from the melt is of major importance in the prediction of the growth rates of various crystal planes, and, eventually, the growth morphology of the crystal as a whole. Except for very large deviations from the melting temperature, where homogeneous nucleation may dominate the dynamics, the process of melting and freezing of a crystal takes place at the interface. Since this interface, being a combination of two dense phases, is not easily accessible to experiment, computer simulations provide a good means to elucidate the microscopic restructuring processes involved in crystallization and melting. In this study, we will use Molecular Dynamics (MD) simulations to look at the growth and melting of the Lennard-Jones (100) interface at small amounts of undercooling and superheating. In this regime, the interface is thermodynamically rough and defect growth does not play a significant role.

One of the first accounts of the steady-state motion of a crystal-melt interface in MD simulations has been the work of Broughton, Gilmer, and Jackson.[1] They combined a solid and a liquid phase in one simulation box and calculated the steady-state velocity of the interface as a function of temperature. A theoretical prediction for this dependence is supplied by the Jackson–Chalmers theory,[2] where the solid–liquid transition is assumed to take place through some intermediate or transition state. The rates R are given by:

$$R(T)=C_1\exp\left(-\frac{Q}{k_BT}\right)\times\left[1-\exp\left(\frac{(h_l-h_s)(T-T_m)}{k_BT\times T_m}\right)\right], \tag{1}$$

where Q is the activation energy for diffusion in the liquid, and h is the enthalpy per particle of the respective phase. Broughton *et al.* showed that for the Lennard-Jones FCC (100) surface, the incorporation of atoms on the surface of the crystal is not an activated process. This led them to replace the Arrhenius factor by a factor proportional to the thermal velocity of the atoms:

$$R(T)=C_2T^{1/2}\left[1-\exp\left(\frac{(h_l-h_s)(T-T_m)}{k_BT\times T_m}\right)\right], \tag{2}$$

which was shown to reproduce their data over a wide range of temperatures (albeit all below T_m). Both Eqs. 1 and 2 lead to the general observation that melting rates are larger than crystallization rates, at equal amounts of supersaturation. This might be one of the reasons that over the past decades a large number of simulation studies have appeared on the freezing of crystals, but comparatively few on melting. For instance, in a successive paper of the Broughton group,[3] they tried to complement their growth studies with melting, but they failed to produce steady state melting. Instead they quickly reached the mechanical melting point, i.e., the point at which the whole crystal disintegrates at once. Note that the undercoolings and superheatings they used are enormous compared to the ones we will look at.

The asymmetry of freezing and melting kinetics was first shown experimentally for crystalline silicon (*c*-Si) growing from amorphous silicon (*a*-Si) by Tsao *et al.*[4] Their results were later reproduced with MD simulations by Kluge and Ray,[5] using a Stillinger–Weber potential, and by Iwamatsu and Horii[6] with classical Density Functional Theory (DFT). Note that, although they all report an asymmetry between melting and freezing in these systems, there is no slope discontinuity of the growth rate versus temperature curve upon crossing the melting point. It was mentioned already in the 1920s, in an Ansatz by Tammann,[7] that such a slope discontinuity cannot occur. This was restated in the 1960s by Uhlmann *et al.*,[8] who argued that an abrupt change in the kinetic coefficient (C_2 in Eq. 2) on going from freezing to melting would imply a violation of microscopic reversibility.

[a]Electronic mail: h.l.tepper@ct.utwente.nl
[b]Electronic mail: w.j.briels@tn.utwente.nl

 © 2001 American Institute of Physics

Downloaded 02 Apr 2009 to 130.89.112.87. Redistribution subject to AIP license or copyright; see http://jcp.aip.org/jcp/copyright.jsp

However, in their study of crystallization and melting of sodium, Tymczak and Ray[9,10] found a clear slope discontinuity at the equilibrium temperature. Singularities at the melting point were subsequently reported with dynamic DFT calculations,[11] a kinetic mean field theory,[12] and lattice gas simulations.[13] The theory of Richards[14] tried to explain the asymmetry on the basis of the density change upon freezing or melting, but the major role of this density change was later contradicted by the work of Oxtoby and Harrowell.[15] Up till now, the question is still under debate.

Recently, we performed nonequilibrium simulations for the FCC (100) interface with the Clarke[16] potential. In that paper[17] we investigated the influence of system size effects and carried out thorough thermodynamic averaging to arrive at very accurate statistics. This initially led to a clear asymmetry of growth and melting rates close to equilibrium, which was attributed to lattice imperfections in the growing crystals. It was shown that if the melting simulations were started with the initially grown crystals, the asymmetry was made to disappear, thus showing it to be an artifact of the simulations. A comparable asymmetry was found in the growth and melting simulations of Huitema *et al.*,[18] but since they were mainly interested in crystallization rates, they did not discuss it.

In an earlier study of ours, we presented a method to extract the temperature dependence of the interface velocities from the fluctuations in an equilibrium simulation.[19] Note that, for the applicability of this efficient method, it is crucial that no slope discontinuity exists at the equilibrium temperature.

In the present study, we will carry out nonequilibrium simulations for a pure Lennard-Jones substance and extend our previous findings. We will demonstrate the crucial importance of good equilibration and we will report on the discovery of two time-regimes of growing and melting rates. The initial regime is associated with interface relaxation, while the second regime is associated with the macroscopic limit of growth. We will discuss the risk that when equilibration is not carried out to full extent, or when too small system sizes are used, only the initial regime will be observed, which can easily lead to erroneous conclusions about the temperature dependence of growth and melting rates. The procedures described here will be of general interest to the study of crystal–liquid interfaces in simple systems, both dynamically and in equilibrium, which continues to be the topic of many theoretical and simulation studies at present.[20–23]

This paper is organized as follows. In the next section, we will describe our simulation system. First we mention how we tuned our thermostat and barostat to carry out the nonequilibrium simulations. Second, we describe the interparticle interactions and pay particular attention to how long-range corrections to the pressure should be carried out in simulations where two phases are present. In Sec. III we describe our equilibration method and show that proper equilibration is crucial to extract the correct rates. The succeeding section deals with the results of the nonequilibrium simulations and the discovery of the two regimes of linear growth rate. Finally, in Sec. V, the temperature dependence of the rates will be presented and it will be shown that, for our system, a slope discontinuity does not exist at the melting point.

II. SIMULATION DETAILS

A. Nosé–Hoover dynamics

In this study, we simulated two-phase crystal-melt systems at constant number of particles (N), pressure (P), and temperature (T). In order to accomplish this, we employed Nosé–Hoover dynamics.[24,25] This scheme is known to have a well-defined conserved quantity and to generate trajectories with the correct distribution of pressures and temperatures. Although thermodynamic properties like pressure and temperature are only rigorously defined as ensemble averages, we will use these terms also to refer to the instantaneous values of their microscopic estimators:

$$\hat{T} = \frac{1}{N_f k_B} \sum_{i=1}^{N} \frac{|\mathbf{p}_i|^2}{m_i} \tag{3}$$

and

$$\hat{P} = \rho k_B \hat{T} + \frac{1}{3V} \sum_{i=1}^{N} \mathbf{r}_i \cdot \mathbf{f}_i , \tag{4}$$

with N_f the number of degrees of freedom.

In the Nosé–Hoover scheme both pressure and temperature are constrained to produce the desired distributions by coupling to a bath by means of parameters that rescale the volume and the particles velocities, respectively. The algorithm has been shown to be quite robust with respect to the speed at which momentum space and configuration space are rescaled.[26,27] However, since we are dealing with systems that are not in thermodynamic equilibrium in this study, we do not only require that the scheme produces the correct distributions on average, but also within reasonable time. More specifically, in the case of a growth simulation, for example, we do not wish the system to have crystallized by a substantial amount before it has sampled a representative part of the temperature and pressure distributions. This additional requirement of fast thermostat and barostat equilibration makes the choice of both the timestep and the bath relaxation times much more delicate than in simulations at thermodynamic equilibrium.

In order to be on the safe side with respect to energy drifts (cf. Ref. 26, Table 2), we used a timestep of $7.480 \times 10^{-4}\ \sqrt{m\sigma^2/\epsilon}$ (reduced Lennard-Jones units) in all our simulations. For tuning of the relaxation times, we studied the distributions of temperature and pressure in both a bulk liquid and a bulk solid of Lennard-Jones particles with a cutoff radius of 2.5 σ and long-range corrections to the pressure and the energy. The distributions were calculated over short runs of 50 000 timesteps after equilibration. The temperature distributions were measured at constant NVT, and the pressure distributions at constant NPT (bulk liquid) or $N\bar{\bar{\sigma}}T$ (bulk solid). Here constant pressure tensor $\bar{\bar{\sigma}}$ means that both the box volume and shape were allowed to relax. Results are shown in Fig. 1. From this figure it can be seen that when a relaxation time is given too small a value, the

Downloaded 02 Apr 2009 to 130.89.112.87. Redistribution subject to AIP license or copyright; see http://jcp.aip.org/jcp/copyright.jsp

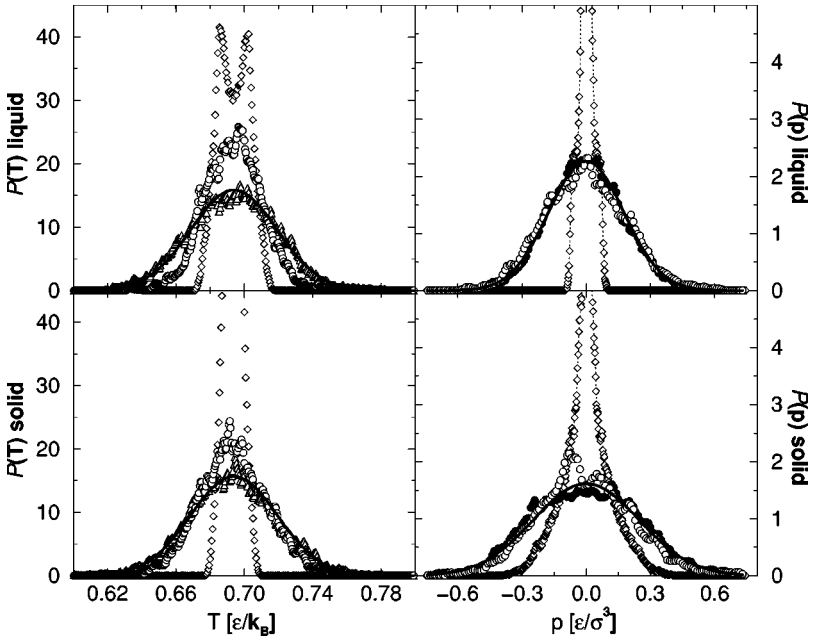

FIG. 1. *Left side:* Normalized distributions (NVT) of the temperature estimator in a bulk liquid (512 atoms) and a bulk solid (500) atoms at $T=0.694\ \epsilon/k_B$. Measurements are taken over 50 000 timesteps for $\tau_T=0.007\,48\ \sqrt{m\sigma^2/\epsilon}$ (diamonds), $\tau_T=0.0748\ \sqrt{m\sigma^2/\epsilon}$ (triangles), and $\tau_T=0.748\ \sqrt{m\sigma^2/\epsilon}$ (circles). The solid lines represent a Gaussian distribution with variance $2T^2/3(N-1)$. *Right side:* Normalized distributions (NPT) of the pressure estimator in a bulk liquid (512 atoms) and a bulk solid (500) atoms at $T=0.694\ \epsilon/k_B$. Measurements are taken over 50 000 timesteps for $\tau_P=0.0748\ \sqrt{m\sigma^2/\epsilon}$ (diamonds), $\tau_P=0.748\ \sqrt{m\sigma^2/\epsilon}$ (triangles), and $\tau_P=7.48\ \sqrt{m\sigma^2/\epsilon}$ (circles). The solid lines represent fits to Gaussian distributions (variances $\sigma_P^{\text{liquid}}=0.031$ and $\sigma_P^{\text{solid}}=0.061$).

corresponding property remains too close to the average value. Also, one can see that there is a steady ''overshoot,'' i.e., the values basically bounce back and forth between two values just below and above the average. From the time evolution (not shown here) it appeared that this process happens at one distinct frequency. On the other side of the spectrum, if relaxation times are chosen too large, the distribution does not have the correct width either, at least not within the 50 000 timesteps displayed here. In the end, the system will sample the whole distribution, but it does so by long-time fluctuations superimposed on the chaotic short-time oscillations (which again was seen from the time evolutions).

We also investigated the temperature distribution in the constant pressure simulations. They were nearly equal to the ones shown here (for NVT simulations), from which we conclude that for our choice of relaxation times, the thermostat and the barostat variables do not interact. For all the simulations in this study, we chose as thermostat relaxation time $\tau_T=0.0748\ \sqrt{m\sigma^2/\epsilon}$ and as barostat relaxation time $\tau_P=0.748\ \sqrt{m\sigma^2/\epsilon}$.

B. The model system

In a previous paper,[17] we used the Clarke 12-6 potential[16] to model particle–particle interactions. This potential has the advantage that it goes smoothly to zero at a predescribed cutoff distance. However, since much more data exist both numerically and theoretically on the simpler Lennard-Jones potential, we chose the latter for the present study. All interparticle interactions were modeled with the standard Lennard-Jones 12-6 potential with a cutoff radius (r_c) of 2.5 σ. Accordingly, all properties in this paper will be presented in terms of the well-depth ϵ, the radius σ and the mass m.

Because the potential is rigorously put to zero beyond the cutoff radius, the long-range tail of the (infinite) potential is missed, which must be corrected for in the energy and the pressure. Such corrections naturally depend on the density of the system. Since in constant pressure simulations the density changes during the run, the corrections must be made at run-time. This is usually done by assuming that the radial distribution function $g(r)$ is approximately equal to 1 for $r>r_c$ and then analytically integrating the interaction potential or the virial contribution (for energy and pressure, respectively) multiplied by the bulk density squared. In a system with two phases of different densities, however, there is no well-defined bulk density, which makes the procedure less straightforward. In the Appendix of this paper, an expression is derived for the long-range correction to the pressure in a system with two phases separated by a flat interface (see Eq. A4). The resulting values for different fractions by volume α of crystalline material are given in Fig. 2. As can be seen from the figure, there is surprisingly little difference between our improved expression and the correction made with the overall density.

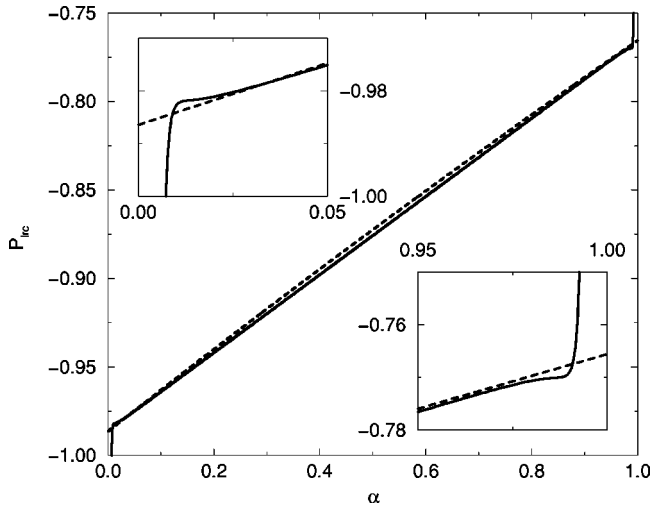

FIG. 2. Long-range corrections to the pressure in a two-phase system as a function of the volume fraction α ($=V_l/V$). Shown are expressions A4 and A6.

Downloaded 02 Apr 2009 to 130.89.112.87. Redistribution subject to AIP license or copyright; see http://jcp.aip.org/jcp/copyright.jsp

It has recently been pointed out by Baidakov *et al.*[28] that in simulations where an interface is present, it can be extremely important to explicitly take into account enough of the long-range interactions. For example in their simulations of the Lennard-Jones liquid–vapor interface, they found extensive changes of thermodynamic properties, the surface tension and the thickness of the interface layer upon going from a small ($2.6\ \sigma$) to a large ($6.78\ \sigma$) cutoff radius. Thus, the asymmetry that was felt by particles due to the presence of the interface extended far into both phases. This would imply that a big difference is to be expected between using our new expressions and rough estimates of long-range corrections, especially since our cutoff radius is not that large. No such differences were observed however. The reason for this may be that liquid–vapor interfaces and crystal–liquid interfaces differ in the density change upon crossing the interface. At least for monatomic systems, this change is quite small for the crystal–liquid interface and comparatively large for the liquid–vapor interface. (In our case $\rho_s/\rho_l=1.135$).

There is another, more pragmatic, problem with our new expression. In order to use it at runtime in a simulation, one has to be able, at every single timestep, to tell the amount of solid and liquid material in the system. For this, we could use our solid–particle recognition criterion (see Ref. 19) but that slightly overestimates the amount of liquid material since it assigns most of the (diffuse) interface to the liquid phase. Another method, which connects more closely to the derivation we used in the Appendix, is to look at the total instantaneous volume of the system. Since we know from our bulk simulations the volumes per particle for each phase, we could at every instance calculate the proportion between solid and liquid phases. This, however, does not work either. Since instantaneous volume fluctuations will also take place in the bulk parts of the two-phase system, our average particle volumes are not a good measure. As a consequence, at certain instances, our prediction for α could exceed 1 or drop below 0. As can be seen from Fig. 2, the new expression diverges close to these values. Any other method that could be suggested to distribute the material over the two phases would suffer from comparable inaccuracies. Since the associated errors are most probably larger than the difference between the two expressions, we decided to keep using the overall average density in calculating instantaneous corrections to the pressure and the energy.

III. EQUILIBRATING THE TWO-PHASE SYSTEM

In our earlier paper,[17] we showed that proper preparation of the two-phase system plays a crucial role in the resulting growth and melting rates. In that paper, we combined fully equilibrated bulk phases of liquid and solid in one simulation box. To release excessive potential energies due to particle overlap, 300 timesteps of NVT simulations were performed with rigid temperature scaling at every timestep. Thereafter, NPT runs were carried out at the appropriate temperatures and $P=2.512\times10^{-3}$ to study growth and melting. We found that the crystals that were grown in the NPT simulations contained just a little more ''imperfections'' (as defined by our solid–liquid discriminator, see Ref. 19) than the crystals that were molten directly after equilibration. This resulted in a clear asymmetry of growth and melting. It was also shown that imperfections eventually appeared in the crystalline phase when the system was run for a long time at the equilibrium temperature, which means that the crystals with imperfections really represent the thermodynamically favored state. It was argued that the crystals lacking imperfections melt more slowly than realistic crystals would do. Indeed, when the crystals grown in the crystallization runs were used for the melting runs, the asymmetry was shown to disappear. Thus, an extensive and careful equilibration of the system at the melting point will most probably also give a symmetric behavior of growth and melting.

In the present study, we chose to perform such a careful equilibration. Like before, we carried out bulk simulations of liquid and solid phases at the appropriate densities, but this time only at the melting temperature. The densities were found by doing several NPT runs of the bulk phases at different temperatures and fitting the average volumes as a function of temperature. For the average volumes per particle this led to (in Lennard-Jones units):

$$v_l=1.0312-0.158\ 02\times T+0.537\ 48\times T^2 \tag{5}$$

and

$$v_s=1.0513-0.340\ 68\times T+0.468\ 30\times T^2, \tag{6}$$

for $0.640<T<0.747$.

First, we needed an estimate of the equilibrium temperature T_m. For this we used the most accurate collection of thermodynamic data for the Lennard-Jones system at this moment, the Johnson data for the liquid[29] and the van der Hoef data for the solid.[30] From these data we calculated the chemical potentials at the desired pressure and sought for the temperature at which the chemical potentials of the solid and the liquid are equal. This gave an estimate of $T_m=0.687$. At this temperature, we performed a two-phase NVT simulation and measured the pressure. Next we slightly changed the temperature until the pressure reached the desired value. From this we found $T_m=0.696\ 59$ and thus, with the above fits, $v_l^{\mathrm{eq}}=1.1819$ and $v_s^{\mathrm{eq}}=1.0412$. At this temperature and pressure, the equations of Johnson and van der Hoef give $v_l=1.1838$ and $v_s=1.0446$, in quite good agreement with our calculations. The agreement of both the melting point and the associated densities is almost perfect, given the fact that for simple systems, the curves of free energies of the two phases versus temperature have very similar slope. Thus a small error in the free energy of one phase with respect to the other leads to a large error in the predicted transition point.

With the densities found above, we performed NVT simulations of the bulk phases at the equilibrium temperature. Here the liquid boxes were elongated along the z-direction and were given the same cross-sectional areas in the x,y-plane as the solid boxes. The bulk simulations were first run for 100 000 timesteps of equilibration, whereafter coordinate files were written once every 1000 timesteps for 50 000 more timesteps in total. To make two-phase boxes, one liquid configuration and one solid configuration were taken, both copied four times in the z-direction, and subsequently put on top of each other. The resulting systems contained two solid–liquid interfaces and consisted of 2000 ini-

Downloaded 02 Apr 2009 to 130.89.112.87. Redistribution subject to AIP license or copyright; see http://jcp.aip.org/jcp/copyright.jsp

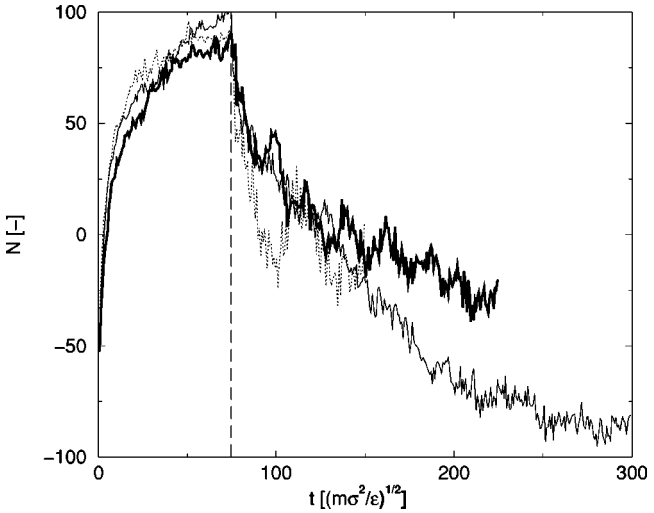

FIG. 3. Increase and decrease of the number of solidlike particles during the equilibration process. Shown are the results for three different box sizes: 4048 particles (thin solid line), 8096 particles (thick solid line), and 16 192 particles (dotted line). The dashed line denotes the point after which the crystal is allowed to relax.

tially crystalline particles ($5\times5\times20$ unit cells) and 2048 particles initially belonging to the liquid phase.

This is the point where the new procedure starts to deviate from the one in the previous study. We used to continue with 300 timesteps of strict temperature scaling to release the particle–particle overlap caused by the combination of the two phases. Upon closer examination, however, it appeared that this had the side effect of removing any ''imperfections'' that were present in the bulk crystal phase. So the imperfections, which belong to a well-equilibrated crystal, disappeared just because of those (very short!) simulations with strict temperature scaling. Therefore we decided to keep the solid phase atoms frozen at their positions and applied 750 timesteps of strict temperature scaling to the liquid only. This proved to be enough to get rid of most of the overlap energies. Thereafter the liquid was equilibrated for 100 000 timesteps, while still constraining the crystal to its original configuration. This way, the liquid was equilibrated against a crystal with the correct amount of imperfections, but with a temperature of essentially zero Kelvin. Therefore, the equilibration should not be extended too long, in order to avoid excessive ''freezing'' of the liquid on the crystalline surface. After the liquid equilibration, the solid was finally relaxed as well and the whole system was run another 300 000 timesteps of equilibration. During the whole procedure, we counted the number of solidlike particles using our recognition function.[19] This was done for 50 runs of different starting configurations and subsequently averaged at each time. We found that this number of 50 runs gave a good trade-off between accuracy and computational cost. We will also discuss this in the next section (Fig. 5).

Results for the averaged equilibration curves are shown in Fig. 3. Apart from the results of the 4048 particle system, curves are also shown for systems of double and quadruple size. In order to monitor processes at the interface, all three curves were shifted downward by the number of solid particles that corresponds to the sizes of the bulk systems that were combined. In the bulk crystal simulations, on average 94.18% of the particles were classified as solid particles by our discriminator. In the bulk liquid simulations, this was 0.058 59%. Accordingly the curve of the small box was shifted down by $0.9418\times2000+0.000\,5859\times2048=1885$ particles. The other curves were shifted by 3770 and 7539 particles, respectively.

All curves start below zero, as a result of the 750 timesteps with strict temperature scaling (not included in the figure) and the fact that particles that ''see'' a crystal on one side and a liquid on the other, will no longer be classified as solidlike. (If it had been only for the latter effect, one would have expected a value of -100, corresponding to 2 interfaces of 50 atoms.) During the equilibration of the liquid against the constrained solid, the amount of crystalline material increases. This happens because a crystal-like interface is built up in the contact region between both phases. After the release of the solid phase, the amount of crystalline material drops again, because of relaxation in the crystalline part of the interface. For the smallest box, equilibrium is only reached after approximately 300 000 timesteps (corresponding to a simulation time of $224.4\sqrt{m\sigma^2/\epsilon}$), which is extremely much larger than most other studies so far have assumed to be sufficient. The two larger boxes need less time to reach equilibrium. Note also that the double and quadruple box seem to converge to approximately the same value of N. We will come back to these observations later when we discuss the system size effects on our production runs.

IV. NONEQUILIBRIUM SIMULATIONS

To carry out production runs of crystallization and melting, the well-equilibrated two-phase systems were quenched to the desired temperatures, by reassigning velocities from a Gaussian distribution with the appropriate mean and width. Then simulations were carried out in the NPT ensemble, with a Nosé–Hoover thermostat and barostat, applying the same parameters as in the bulk simulations (Sec. II A). The barostat was adopted such that the volume relaxation in the x-, y-, and z-directions took place independently. The production runs were again carried out over 50 independent starting configurations (the end configurations of the equilibration runs) at each temperature. During the runs, the number of crystalline particles was calculated once every 100 timesteps. Results of the 50 runs were subsequently averaged.

One example of an averaged melting run is shown in Fig. 4. To investigate the influence of equilibration time, we started melting runs from three different stages in the equilibration (100, 200, and 300 thousand timesteps after the release of the crystal phase). All three cases show an initial rapid drop of the number of crystalline particles. This reflects the relaxation of the system to the new temperature. Simultaneously, the volume of the box increased by a corresponding amount. After this short period, the (averaged) temperature and pressure had relaxed to their desired values.

Shortly after the initial box relaxation, the system started to melt with a constant velocity in all three cases. The experiment with the shortest equilibration time melted somewhat slower than the two others. A remarkable feature, how-

Downloaded 02 Apr 2009 to 130.89.112.87. Redistribution subject to AIP license or copyright; see http://jcp.aip.org/jcp/copyright.jsp

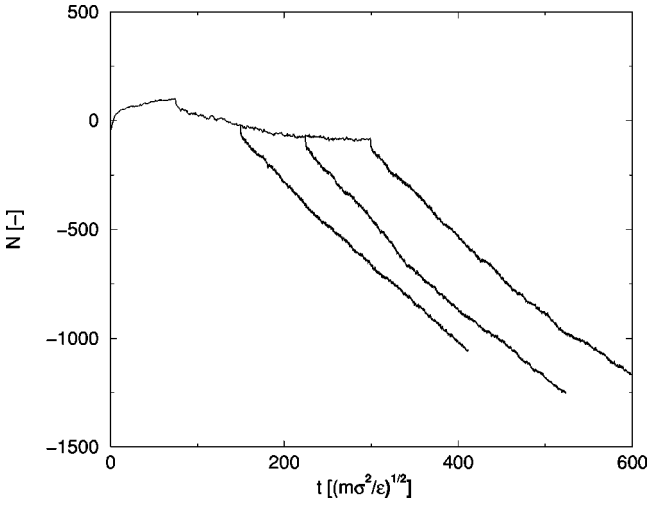

FIG. 4. Melting curves at $T=0.714\ \epsilon/k_B$ started from three different stages in the equilibration process.

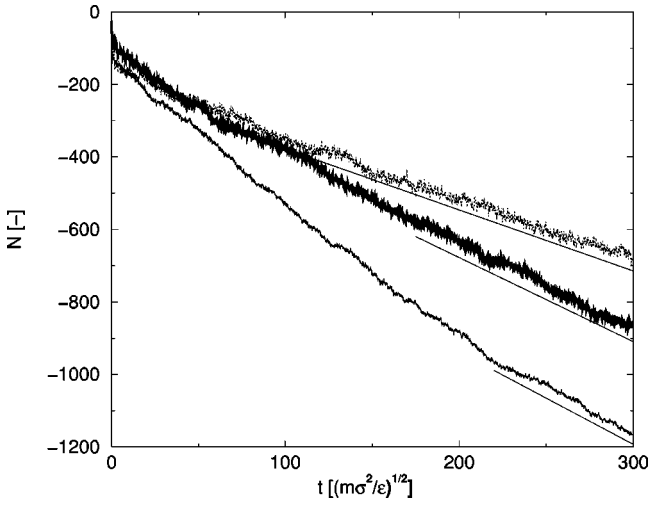

FIG. 6. Averaged melting curves at $T=0.714\ \epsilon/k_B$ for different box sizes with a total number of particles of 4048 (50 runs, thin solid line), 8096 (50 runs, thick solid line), and 16 192 (32 runs, dotted line), respectively. Clearly shown is the good agreement of both the initial and the final slopes of the different experiments.

ever, of all three cases, is that they displayed a second regime, where the melting was again linear in time but took place at a smaller rate than initially. This crossover from an initial to a second regime was clearly noticeable for most of the temperatures at which we performed our measurements, though less pronounced for the crystallization runs than for the melting runs and less pronounced for temperatures very close to equilibrium. Note, however, that the effect is also quite subtle: in order for the effect to be seen, it is necessary to carry out averaging over many different runs. This is shown in Fig. 5, where a selection of single runs is drawn together with the curve averaged over all 50 boxes. On the temperature range that we study, the fluctuations of N_s in one single run are of the same order as the differences between the averaged curves of different temperatures.

The discovery of two distinct regimes of growth and melting raises two questions: *"Is this an artifact of the simulation method (e.g., an effect of system size), or is it a real, physical effect?"* and *"If it is not an artifact, which one of the two regimes corresponds to the rates that are to be associated with macroscopic crystal growth such as would be seen in experiments?"*

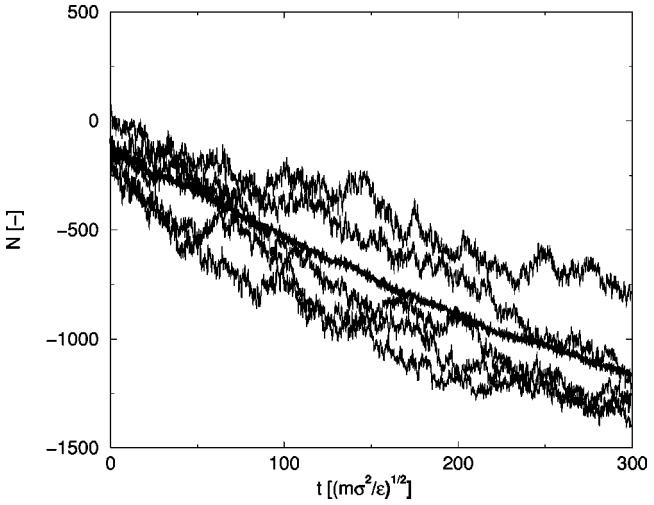

FIG. 5. Melting curves at $T=0.714\ \epsilon/k_B$ showing a selection (5 runs) from different starting configurations, as well as the average over 50 runs (broad line).

In order to study system size effects, we repeated our simulations for systems of twice and four times the original sizes. We could have constructed the new two-phase boxes by taking 8 or 16 periodic images of the bulk phases (instead of 4 for our smaller system). However, we chose to do the bulk (NVT) simulations anew at the actual sizes that we needed in the two-phase simulations. In this way, we made sure that we combined two completely randomized phases and did not introduce any undesired periodicity. (In a previous study of ours,[31] where we studied density fluctuations of adsorbed species in nanopores, we learned that in order to sample long-wavelength fluctuations of the order of the box size, one has to completely randomize initial positions of the particles over the whole pore. There it proved not to be sufficient, say, to divide the pores in four sections of equal length and distribute a fourth of the particles randomly over each of the sections). To summarize, the two-phase systems of 8096 particles were constructed from bulk liquids of 4096 particles and bulk solids of 4000 particles, and the two-phase systems of 16 192 particles were constructed from bulk phases of 8192 and 8000 liquid and solid particles, respectively.

The resulting averaged curves for the same temperature as in Fig. 5 are shown in Fig. 6. The most striking feature of this graph is that all three curves seem to start with the same initial slope and to end with approximately equal slopes as well. Only the time over which the initial regime extends seems to shorten substantially with increasing box size. We suggest that both regimes belong to a physical process, which is reflected by the fact that neither slope does change significantly upon enlarging the box size. Since the second regime seems to be persistent and becomes increasingly dominant when the system is enlarged, we infer that this regime is to be associated with the macroscopic limit of crys-

Downloaded 02 Apr 2009 to 130.89.112.87. Redistribution subject to AIP license or copyright; see http://jcp.aip.org/jcp/copyright.jsp

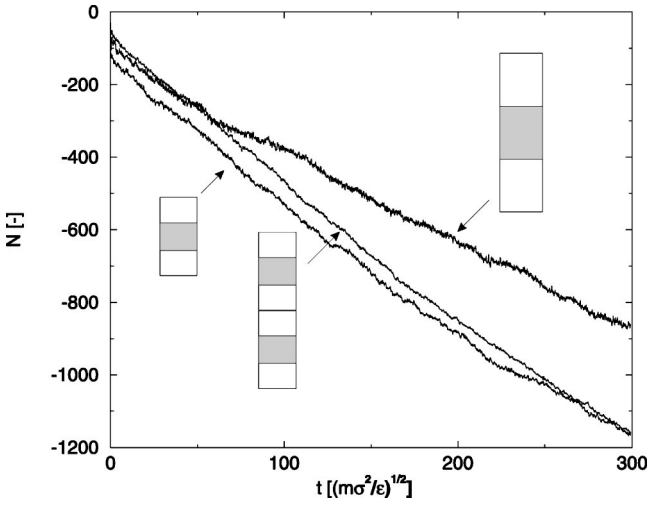

FIG. 7. Comparison of melting curves for the small and intermediate box sizes, where either both phases are doubled or the whole system is copied twice.

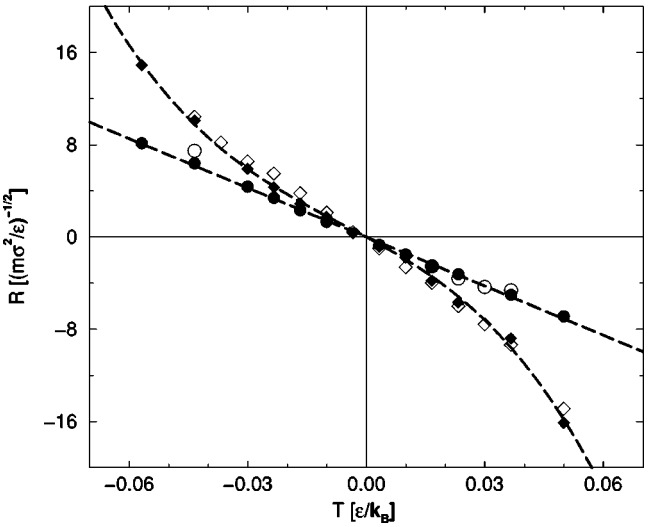

FIG. 8. Dependence upon the supersaturation (deviation of the temperature from equilibrium) of the initial (pyramids) and long-time (circles) growth and melting rates. Shown are the results for the small (open symbols) and intermediate (closed symbols) box sizes.

tal growth (or melting). As can be seen from the figure, the slope of the second regime still changed somewhat upon enlarging the size, but for computational reasons we decided the results of the intermediate boxes were converged satisfactorily (this was a generic trend for all temperatures).

The initial regime may be a relaxation of the interface reflecting a change from the equilibrium shape at the melting point to a steady-state shape belonging to the actual temperature of the experiment. This is in accordance with kinetic mean field results of Williams, Moss, and Harrowell.[12]

One might argue that if local density fluctuations are crucial and only the total number of particles in the simulation plays a role in the size of these fluctuations, the effect should also be seen in a system that is built as two copies of the original box (thus containing four interfaces per simulation cell). This we checked by comparing the results from the small box with those from the intermediate box and those from a system that was made by copying the small box twice in the *z*-direction. The results are shown in Fig. 7. One can see that the larger fluctuations in the ''doubled small'' box give ease to a better buildup of the equilibrium interface (reflected in the starting point of the melt run which is close to that of the large box). In the nonequilibrium situation, however, the long-time behavior is close to that of the small box. Thus it is really the bulky behavior of the large phases in the larger box that makes the interface relax to its nonequilibrium shape. Note again that our ''small'' system is of comparable size or larger than the maximum system sizes of most other studies. This means that those studies probably have been investigating interface relaxation rates rather than macroscopic crystal growth rates.

A second concern that might be raised is that immediately after the initial quench, the crystal starts to grow (or melt) thereby releasing (consuming) latent heat of fusion. If the thermostat would not be able to remove all of the extra heat, the interface may heat up (cool down) until balance is reached between heat production and heat transport. This effect would slow down both growth and melting rates, since the final temperature at the interface would then be closer to the melting point than the overall temperature. In order to investigate this, we did a thorough study of temperature profiles by monitoring local averages of the kinetic energy, both averaged over the whole run and followed as time evolution. In neither case did we find any noticeable deviation of the interface temperature from the overall temperature. From this we conclude that our thermostat relaxation time was chosen small enough so as to effectively produce constant temperature experiments.

V. TEMPERATURE DEPENDENCE OF GROWTH AND MELTING RATES

We carried out simulations with the small and intermediate boxes at several different temperatures below and above the equilibrium temperature. For all experiments, averages were calculated over 50 different initial configurations. The small box systems were equilibrated over 100 000 timesteps with frozen crystal configurations and 300 000 timesteps with the whole system relaxed, while the intermediate box systems were equilibrated over 100 000 steps with a frozen crystal and 200 000 steps with both phases relaxed. For the small systems, the initial slopes were calculated easily, but the second regime was only accurately measured in one growth and four melting experiments. The reason for this was that close to equilibrium, the second regime was not found, and far from equilibrium, there was only a very short time of second regime (if any) before the system had grown one of the two phases so far that the two interfaces in the box started to interact. Most of the intermediate size experiments showed both regimes over a substantial time. The results are shown in Fig. 8. It can be seen that over the whole range of temperatures studied, the agreement between both system sizes is good. The long-time regime rates are perfectly linear with respect to temperature. We think that this is clear evidence of the Ansatz of Tammann[7] and supplies an extra confirmation of the fact that the long-time regime is indeed to be associated with the macroscopic limit of growth and melting.

Downloaded 02 Apr 2009 to 130.89.112.87. Redistribution subject to AIP license or copyright; see http://jcp.aip.org/jcp/copyright.jsp

The initial rates are not linear in temperature. This implies that improper equilibration might be one of the reasons why earlier researchers (including ourselves) have found nonlinearities or slope-discontinuities around equilibrium in the dependence of growth rates upon under- and supersaturation, even for roughly growing surfaces.

Finally, we investigated the dependence of the crossover time between the two regimes upon temperature. We started to make a linear fit through the second-regime growth rates (denoted by R_2). This resulted in:

$$R_2^{\mathrm{fit}}(T) = 99.052 - 142.07\,T. \tag{7}$$

Note that this leads to a definitive estimate of the equilibrium temperature for our system of $T_m = 0.6972\epsilon/k_B$, in very close agreement with our earlier estimate. Next we fitted the initial-regime growth rates with a third order polynomial in ΔT (the deviation of the temperature from equilibrium). This resulted in

$$R_1^{\mathrm{fit}}(T) = -184.19\,\Delta T - 739.39\,\Delta T^2 - 38291\,\Delta T^3. \tag{8}$$

The accuracies of these fit can be appreciated from Fig. 8.

Now, for each experiment, we did not only measure the slopes of the growth curves, but also the intercepts with the N-axis. We fitted the intercepts (denoted A) of the initial regimes with a third-order polynomial in ΔT:

$$A_1^{\mathrm{fit}} = -10.2 - 3850.4\,\Delta T - 17694\,\Delta T^2 + 1.2236\times 10^5\,\Delta T^3. \tag{9}$$

Next we fitted the intercepts of the second regimes, while constraining the zeroth order term to the value of the initial intercepts. This means forcing both curves to coincide at equilibrium ($\Delta T = 0$):

$$A_2^{\mathrm{fit}} = -10.2 - 6443.4\,\Delta T - 39576\,\Delta T^2 - 1.8772\times 10^5\,\Delta T^3. \tag{10}$$

The results are shown in Fig. 9. The difference between A_1^{fit} and A_2^{fit} can be interpreted as a measure for the difference between the widths of the nonequilibrium interface and the equilibrium interface. The points at which both fits $A_i^{\mathrm{fit}} + R_i^{\mathrm{fit}} \times t$ intersect are our estimates for the crossover times:

$$t_{\mathrm{cross}} = \frac{2593.0 + 21\,882\,\Delta T + 3.1008\times 10^5\,\Delta T^2}{42.12 + 739.39\,\Delta T + 38\,291\,\Delta T^2}. \tag{11}$$

In Fig. 10, we have drawn all growth and melting curves for the intermediate box size, including the fits to the linear regimes as well as Eq. 11. As can be clearly seen, the crossover time grows large upon approaching equilibrium, while at the same time the initial and the second-regime rates grow more and more equal.

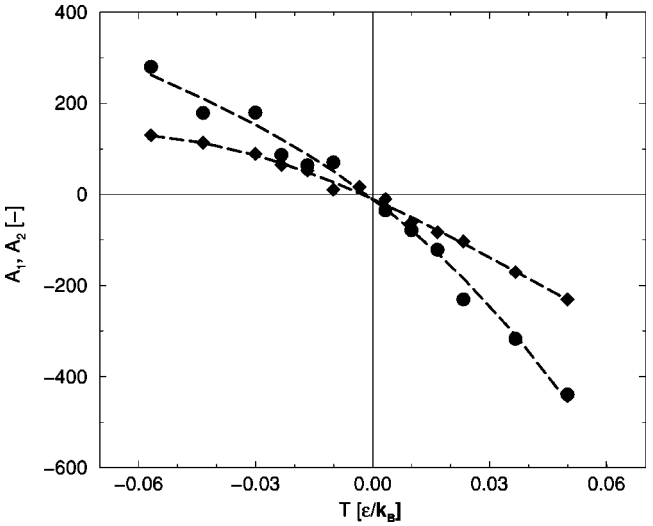

FIG. 9. Temperature dependence of intercepts A_1 (diamonds) and A_2 (circles) of the growth and melting curves. The dashed lines represent the fits of Eqs. 9 and 10.

VI. CONCLUSIONS

We presented the most accurate simulations to date of crystal growth and melting rates of the Lennard-Jones (100) face at temperatures close to equilibrium. We proposed a way to carefully equilibrate two-phase systems to carry out subsequent nonequilibrium simulations and showed that our solid–liquid recognition function supplies a powerful tool to monitor the equilibration process.

We discovered two linear regimes. The initial regime was associated with interface relaxation and was shown to be most dominant for small system sizes and close to equilibrium. The second regime was associated with the macroscopic limit of growth and melting. The linear dependence of the macroscopic rates upon temperature provides clear evidence of the early observation of Tammann that roughly growing surfaces with one type of interaction sites cannot have a slope discontinuity in the rate-temperature curve. This contrasts some earlier simulation studies. We showed that improper equilibration of the two-phase systems can result in the observation of only the initial (interface relaxation) regimes. Since these were shown not to vary linearly with

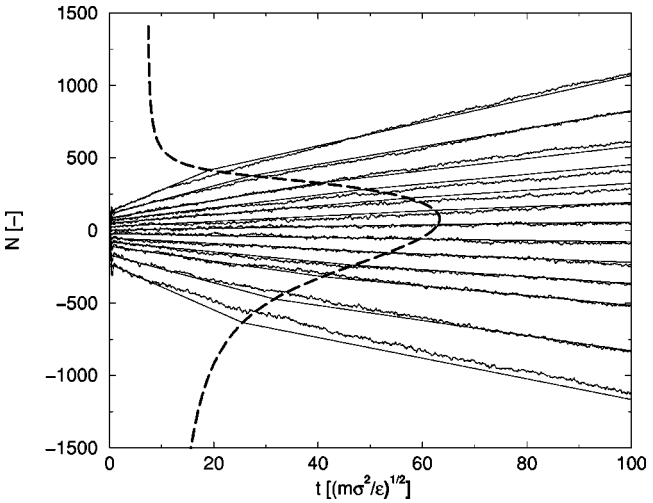

FIG. 10. Growth and melting curves for all temperature at intermediate box size, showing both the measurement data and the fits to the initial and final slopes. The dashed line shows the calculated crossover times between both regimes.

Downloaded 02 Apr 2009 to 130.89.112.87. Redistribution subject to AIP license or copyright; see http://jcp.aip.org/jcp/copyright.jsp

temperature, some (or all) of the earlier observations of a slope discontinuity may be explained by this.

Now that the necessary hardware requirements have come into reach, it has become possible to study the effect of system size and simulation times upon dynamic measurements of two-phase systems. The present study proves that both of these have to be (much) larger than generally accepted in order to arrive at the correct rates. This reflects the fact that the interface present in two-phase systems has an effective interaction range that is apparently much larger than any measure of the interface width would suggest. We think this study provides a good guideline to what dimensions should be used in these systems and may be a suitable starting point to study crystal-melt systems of more complex molecules, where the molecular correlation lengths are already much larger.

APPENDIX A: LONG-RANGE CORRECTIONS TO THE PRESSURE IN A TWO-PHASE LENNARD-JONES SYSTEM

In this Appendix, we derive an expression for the long-range correction to the pressure in a system where two phases are present. We restrict ourselves to the case of a pure substance (the interactions between all particles are identical), the only difference between the two phases being their respective densities. We write the pressure as $-1/6\ V$ times a double integral over space of the densities at two positions $\mathbf{r}_1$ and $\mathbf{r}_2$ multiplied by the virial function w, whose value depends on the distance r between $\mathbf{r}_1$ and $\mathbf{r}_2$. In the case of simple Lennard-Jones particles, this function reads:

$$w(r)=r\frac{d\phi^{\mathrm{LJ}}}{dr}=-\frac{48}{r^{12}}+\frac{24}{r^{6}}. \tag{A1}$$

In the integral, position $\mathbf{r}_1$ probes all material in the simulation box, so this coordinate is restricted to the box volume V, while the second coordinate represents all of the surroundings of the first one and thus, in principle, extends over infinite space:

$$P=-\frac{1}{6V}\int_V d\mathbf{r}_1\int_\infty d\mathbf{r}_2\rho(\mathbf{r}_1)\rho(\mathbf{r}_2)w(|\mathbf{r}_2-\mathbf{r}_1|). \tag{A2}$$

Note that in the calculation of the ''uncorrected'' pressure, the integral reduces to a double sum over nearest images, since all interactions beyond the cutoff radius are zero and box dimensions should be such that non-nearest images are more than r_c apart.

For the construction of the long-range correction, we apply the usual assumption[32] that beyond the cutoff radius, the central particle only ''sees'' average surroundings [which for a pure substance comes down to assuming $g(r)=1$ for $r>r_c$]. Because of this assumption, we may substitute the average densities of the respective phases for $\rho(r)$, where the choice for either ρ_l or ρ_s depends on the region of the corresponding integral. Since there are two different phases, that can appear in four combinations, the long-range correction to the pressure can be split into four distinct integrals:

$$\begin{aligned}
P_{\mathrm{lrc}}=&-\frac{1}{6V}L_xL_y\rho_l\int_0^{\alpha L_z}dz_1\Bigg\{\int_{-\infty}^{+\infty}dx_2\int_{-\infty}^{+\infty}dy_2\\
&\times\int_0^{+\infty}dz_2\rho_l w(|\mathbf{r}_2-\mathbf{r}_1|)\Theta(|\mathbf{r}_2-\mathbf{r}_1|-r_c)+\int_{-\infty}^{+\infty}dx_2\int_{-\infty}^{+\infty}dy_2\int_{-\infty}^{0}dz_2\rho_s w(|\mathbf{r}_2-\mathbf{r}_1|)\Theta(|\mathbf{r}_2-\mathbf{r}_1|-r_c)\Bigg\}\\
&-\frac{1}{6V}L_xL_y\rho_s\int_{-(1-\alpha)L_z}^{0}dz_1\Bigg\{\int_{-\infty}^{+\infty}dx_2\int_{-\infty}^{+\infty}dy_2\int_{0}^{+\infty}dz_2\rho_l w(|\mathbf{r}_2-\mathbf{r}_1|)\Theta(|\mathbf{r}_2-\mathbf{r}_1|-r_c)\\
&+\int_{-\infty}^{+\infty}dx_2\int_{-\infty}^{+\infty}dy_2\int_{-\infty}^{0}dz_2\rho_s w(|\mathbf{r}_2-\mathbf{r}_1|)\Theta(|\mathbf{r}_2-\mathbf{r}_1|-r_c)\Bigg\},
\end{aligned} \tag{A3}$$

where the unit step function Θ is used to denote that only the region outside the cutoff range is taken into account. The integration space covered by the above expression is schematically drawn in Fig. 11.

If we take the further (legitimate) assumption that r_c is smaller than the length of either of the two phases along the z-direction, the above expression can be elaborated upon to give

$$\begin{aligned}
P_{\mathrm{lrc}}=&-\pi\rho_l^2\Bigg\{\left(\frac{16}{3}\alpha-2\beta+\frac{\beta^3}{3\alpha^2}\right)\frac{1}{r_c^3}-\left(\frac{32}{9}\alpha-\beta+\frac{\beta^9}{45\alpha^8}\right)\frac{1}{r_c^9}\Bigg\}-\pi\rho_l\rho_s\Bigg\{\left(4\beta-\frac{\beta^3}{3\alpha^2}-\frac{\beta^3}{3(1-\alpha)^2}\right)\frac{1}{r_c^3}\\
&-\left(2\beta-\frac{\beta^9}{45\alpha^8}-\frac{\beta^9}{45(1-\alpha)^8}\right)\frac{1}{r_c^9}\Bigg\}-\pi\rho_s^2\Bigg\{\left(\frac{16}{3}(1-\alpha)-2\beta+\frac{\beta^3}{3(1-\alpha)^2}\right)\frac{1}{r_c^3}-\left(\frac{32}{9}(1-\alpha)-\beta+\frac{\beta^9}{45(1-\alpha)^8}\right)\frac{1}{r_c^9}\Bigg\},
\end{aligned} \tag{A4}$$

Downloaded 02 Apr 2009 to 130.89.112.87. Redistribution subject to AIP license or copyright; see http://jcp.aip.org/jcp/copyright.jsp

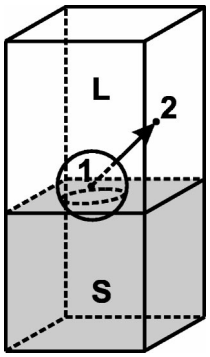

FIG. 11. Sketch of the integration space as meant in Eq. (A3). Position 1 traverses the whole simulation box while position 2 traverses infinite space. The drawn sphere denotes the volume within a radius r_c of position 1, which is excluded from the integral by means of the unit step function Θ.

where we have used the following substitutions:

$$\alpha = V_l/V = 1 - V_s/V,$$
$$\beta = r_c/L_z. \tag{A5}$$

The expression that has been found should be checked to give known results in limiting cases. The most obvious one is to take the densities of the two phases equal ($\rho_l = \rho_s$). This leads to

$$P_{\mathrm{lrc}} = -\pi\rho^2\left(\frac{16}{3}\frac{1}{r_c^3} - \frac{32}{9}\frac{1}{r_c^9}\right), \tag{A6}$$

which is equal to the well-known expression for the long-range correction to the pressure in a pure Lennard-Jones substance.[32]

Another limit that could be looked at is the limit of infinite system size ($L_z \to \infty$, and thus $\beta \to 0$). In that limit the influence of the interface should become unimportant. The resulting expression is

$$P_{\mathrm{lrc}} = -[\alpha\pi\rho_l^2 + (1-\alpha)\pi\rho_s^2]\left(\frac{16}{3}\frac{1}{r_c^3} - \frac{32}{9}\frac{1}{r_c^9}\right), \tag{A7}$$

which can be seen as the analogue of Eq. (A6), but in this case a squarely weighted average of the densities shows up. This is because the density appears as a square in the pressure expression.

It is instructive to see what would happen if one would just use the standard long-range corrections. This comes down to neglecting the situation of two different phases and just taking the number average density of the system as a whole:

$$\bar{\rho} = \frac{N_l + N_s}{V} = \rho_l\frac{V_l}{V} + \rho_s\frac{V_s}{V}$$
$$= \alpha\rho_l + (1-\alpha)\rho_s. \tag{A8}$$

This leads to

$$P_{\mathrm{lrc}} = -\pi[\alpha\rho_l + (1-\alpha)\rho_s]^2\left(\frac{16}{3}\frac{1}{r_c^3} - \frac{32}{9}\frac{1}{r_c^9}\right). \tag{A9}$$

Note the subtle difference with expression (A7).

[1] J. Q. Broughton, G. H. Gilmer, and K. A. Jackson, Phys. Rev. Lett. **49**, 1496 (1982).
[2] K. A. Jackson and B. Chalmers, Can. J. Phys. **34**, 473 (1956).
[3] E. Burke, J. Q. Broughton, and G. H. Gilmer, J. Chem. Phys. **89**, 1030 (1988).
[4] J. Y. Tsao, M. J. Aziz, M. O. Thompson, and P. S. Peercy, Phys. Rev. Lett. **56**, 2712 (1986).
[5] M. D. Kluge and J. R. Ray, Phys. Rev. B **39**, 1738 (1989).
[6] M. Iwamatsu and K. Horii, Phys. Lett. A **214**, 71 (1996).
[7] G. Tammann, *Aggregatzustände* (Leopold Voss, Leipzig, 1923), Chap. 9.
[8] D. R. Uhlmann, J. F. Hays, and D. Turnbull, Phys. Chem. Glasses **8**, 1 (1967).
[9] C. J. Tymczak and J. R. Ray, Phys. Rev. Lett. **64**, 1278 (1990).
[10] C. J. Tymczak and J. R. Ray, J. Chem. Phys. **92**, 7520 (1990).
[11] Y. C. Shen and D. W. Oxtoby, J. Chem. Phys. **104**, 4233 (1996).
[12] A. Williams, R. Moss, and P. Harrowell, J. Chem. Phys. **99**, 3998 (1993).
[13] R. Moss and P. Harrowell, J. Chem. Phys. **100**, 7630 (1994).
[14] P. M. Richards, Phys. Rev. B **38**, 2727 (1988).
[15] D. W. Oxtoby and P. R. Harrowell, J. Chem. Phys. **96**, 3834 (1992).
[16] J. H. R. Clarke, W. Smith, and L. V. Woodcock, J. Chem. Phys. **84**, 2290 (1986).
[17] H. L. Tepper and W. J. Briels, J. Cryst. Growth **230**, 270 (2001).
[18] H. E. A. Huitema, M. J. Vlot, and J. P. van der Eerden, J. Chem. Phys. **111**, 4714 (1999).
[19] W. J. Briels and H. L. Tepper, Phys. Rev. Lett. **79**, 5074 (1997).
[20] B. J. Jesson and P. A. Madden, J. Chem. Phys. **113**, 5935 (2000).
[21] T. Motooka, K. Nisihira, S. Munetoh, K. Moriguchi, and A. Shintani, Phys. Rev. B **61**, 8537 (2000).
[22] J. A. Hayward and A. D. J. Haymet, J. Chem. Phys. **114**, 3713 (2001).
[23] C. S. Liu, J. Xia, Z. G. Zhu, and D. Y. Sun, J. Chem. Phys. **114**, 7506 (2001).
[24] S. Nosé, J. Chem. Phys. **81**, 511 (1984).
[25] W. G. Hoover, Phys. Rev. A **31**, 1695 (1985).
[26] S. Toxvaerd, Mol. Phys. **72**, 159 (1991).
[27] S. Toxvaerd, Phys. Rev. E **47**, 343 (1993).
[28] V. G. Baidakov, G. G. Chernykh, and S. P. Protsenko, Chem. Phys. Lett. **321**, 315 (2000).
[29] J. K. Johnson, J. A. Zollweg, and K. E. Gubbins, Mol. Phys. **78**, 591 (1993).
[30] M. A. van der Hoef , J. Chem. Phys. **113**, 8142 (2000).
[31] J. P. Hoogenboom, H. L. Tepper, N. F. A. van der Vegt, and W. J. Briels, J. Chem. Phys. **113**, 6875 (2000).
[32] M. P. Allen and D. J. Tildesley, *Computer Simulation of Liquids* (Oxford University Press, Oxford, 1987).

Downloaded 02 Apr 2009 to 130.89.112.87. Redistribution subject to AIP license or copyright; see http://jcp.aip.org/jcp/copyright.jsp